Mechanochemical Reactions in Cu/ZnO Catalysts Induced by Mechanical Milling

Hessel L. Castricum,*,† Hans Bakker,† Bart van der Linden,‡ and Eduard K. Poels‡

van der Waals-Zeeman Instituut, Faculty of Science, Universiteit van Amsterdam, Valckenierstraat 65, 1018 XE Amsterdam, The Netherlands, and Department of Chemical Engineering, Universiteit van Amsterdam, Nieuwe Achtergracht 166, 1018 WV Amsterdam, The Netherlands

Received: December 6, 2000; In Final Form: May 7, 2001

Preparation of Cu/ZnO catalysts is discussed in which mechanochemical reactions are involved. These reactions include oxidation of copper and copper oxides during milling in the presence of oxygen, reduction under vacuum, and formation of carbonates in CO_2. Oxidation and reduction are promoted by the presence of ZnO. Formation of Cu_2O-like intermediates is suggested in oxidic mixtures, which are not observed when milling occurs without ZnO. This effect may be partly due to defect formation. The various resulting copper species reduce at different temperatures in H_2 atmosphere and this gives an indication for the intimacy of the Cu−Zn interaction. When milling is carried out in the presence of CO_2, mixed carbonates are formed. Intimate mixtures of Cu and Zn are thus obtained, exhibiting high surface areas after reduction that can be explained by evolved porosity. A linear relation between Cu^0 surface area and activity for methanol synthesis at 2 bar is observed. Irreversible deactivation is explained by over-reduction and sintering. Both Cu^0 specific surfaces and BET surfaces (determined after reduction in hydrogen) are substantially increased for all milled Cu/ZnO samples, but especially for samples that undergo mechanochemical reactions. This method thus allows investigation of mixed oxide catalyst precursors and provides an interesting alternative for the preparation of promoted heterogeneous catalysts.

Introduction

Copper-containing catalysts are widely used in industry for the hydrogenation and dehydrogenation of organic functional groups. Synthesis of methanol from synthesis gas is one of the main applications. Due to its large and still increasing industrial importance, this has become one of the best studied systems in heterogeneous catalysis. On the other hand, despite decades of research controversy still exists about the active site for methanol synthesis.[1−3] Consensus has been reached in the literature that a high activity can be obtained by an intimate mixture of Cu and ZnO (or Cu−Zn−Al/Cr).[4,5] This is the reason that a Cu/ZnO catalyst is conventionally prepared by coprecipitation of $Cu(NO_3)_2$ and $Zn(NO_3)_2$ solutions with subsequent aging and calcination. Mechanochemical preparation of this catalytic system has been introduced in a previous paper[6] as a novel technique for obtaining such a well-mixed system. It offers a promising route for detailed study of mixed oxide catalysts or catalyst precursors.

Mechanochemical reactions can be driven by mechanical milling, which has long been known as a technique for refining particles of solid materials. Most effects that are due to milling can directly or indirectly be attributed to the production of various defects combined with high local temperatures. In pre-alloyed intermetallic compounds, atomic disorder is thus created which can eventually give rise to phase transformations.[7] Other factors playing a role during milling, notably mixing on a microscopic level and formation of a fresh surface, are enhanced by the increase of defects. These underlie mechanical alloying, i.e., creation of a metallic alloy starting from a mixture of elemental powders, and mechanochemistry.

The most common mechanochemical reactions include solid−solid and solid−gas reactions. An example of a reaction between solids is the reduction of metal oxides in the presence of a strong reducing element,[8,9] such as the reduction of CuO in the presence of Ca. Reactions between solids and a gas include the formation of hydrides, nitrides, and oxides.[10−13] Hard materials can thus be prepared such as TiN. Similarly, preparation of catalysts can be performed by mechanical milling due to various interactions between the solids and the gases present in the vial. In this way, vanadium-containing catalysts,[14] CeO_2-based catalysts[15] and Cu/ZnO catalysts can be prepared.

During mechanical milling, the surrounding atmosphere plays a crucial role in the ultimate structure and activity of the catalyst for the reaction of synthesis gas toward methanol. A mixture of Cu and ZnO milled under vacuum appeared to be hardly active, whereas this mixture milled in ambient air was as active as a coprecipitated catalyst.[6] Special attention should also be given to the milling equipment: a considerable contamination with Fe may affect the selectivity toward methanol synthesis, as was shown with mechanochemically prepared supported Cu/ZnO catalysts using different milling equipment.[16]

In this paper, the structure of Cu/ZnO catalysts is studied by systematic variation of precursors and milling atmospheres. Except assessing the mechanochemical reactions that take place and characterizing the structure of the materials, we attempt to determine the conditions under which an active catalyst can be obtained. For reasons of simplicity, we have chosen a binary catalyst instead of the Al_2O_3-supported ternary catalyst that is commonly used in industry. Moreover, the unreduced binary system has a more homogeneous composition, which is convenient for preparation by mechanical milling and leads to

* Author to whom correspondence should be addressed. Tel: (+31) 20 5255991. Fax: (+31) 20 5255788. E-mail: castric@science.uva.nl.

† van der Waals-Zeeman Instituut, Faculty of Science, Universiteit van Amsterdam

‡ Department of Chemical Engineering, Universiteit van Amsterdam

10.1021/jp004394s CCC: $20.00
Published on Web 07/31/2001

a well-defined mixture. We have chosen to use a Cu-to-Zn atomic ratio of 30:70, which yields a catalyst with optimum activity.[17,18] The mechanochemical processes that occur during preparation of milled Cu/ZnO catalysts are studied by comparing them to reactions that occur when only Cu, Cu oxides, or ZnO are involved. The reactions, including reduction, oxidation, and carbonate formation, are examined by milling under vacuum and in the presence of oxygen and carbon dioxide, and were partly discussed earlier in a different framework.[19,20]

Experimental Section

All samples were milled in a vibratory mill[7] attached to a vacuum pump. The vial was typically loaded by 2 g of material. The standard milling time was 200 h for all samples. We used powders of Cu (40 μm, 99.5% pure), Cu_2O (<74 μm, 99% pure), CuO (<74 μm, 99.9% pure), and ZnO (<74 μm, 99.995% pure), all purchased from CERAC. For all mixtures, the Cu-to-Zn atomic ratio was 30:70. In case milling was carried out under vacuum, the pressure was lower than 10^{-6} mbar during continuous pumping. Milling in synthetic air (20% O_2 in N_2, 99.999% pure) and carbon dioxide (99.998% pure) took place at a total pressure of 2 bar after evacuation, filling the vial with this gas and again evacuation to 10^{-6} mbar. When a mixture of synthetic air and CO_2 was used, O_2 and CO_2 partial pressures were set approximately equal (0.4 bar). Ambient air was not considered because of climatic variations, e.g., variation of the water-vapor content.

Cu^0 specific surface areas were determined by N_2O chemisorption according to the method described by means of Thermogravimetric Analysis (TGA) in a Setaram TG 85 thermobalance.[21] The subsurface contribution was subtracted by linear back-extrapolation of the part of the weight curve between 5000 and 10000 s. As polycrystalline Cu was assumed for all samples, an average value of 1.46×10^{19} Cu atoms/m^2 was taken, and a Cu/O stoichiometry of 2. Prior to the chemisorption experiments, the samples were pretreated in an Ar flow (99.999% pure at 120 mL/min) by heating at 200 K/h up to 508 K and then at 100 K/h up to 523 K. After cooling in Ar to ambient, reduction was performed by heating in H_2/Ar (at a ratio of 2:1; total flow: 120 mL/min; hydrogen purity: 99.996%) at 200 K/h to 523 K. This temperature was held during 30 min when milling had been performed in the presence of CO_2, for all other samples it was held during 5 min. Reduction patterns were determined by recording the calibrated sample weight loss during catalyst reduction. N_2O chemisorption took place at 363 K, after cooling and subsequent evacuation at this temperature. The thermobalance was attached to a mass spectrometer, enabling analysis of the molecular weight of the molecules that were released or produced during pretreatment and reduction. The error in Cu^0 specific surface areas is about 1 m^2/g, for high surface areas it is 5−10%.

Total surface areas were determined by the BET-method (N_2 physisorption). All Cu-containing samples were pretreated in a He flow (99.996% pure) at 100 mL/min and reduced in He/H_2 (2/1, total flow: 100 mL/min; hydrogen purity: 99.999%), using a temperature program identical to that used for TGA. ZnO samples were dried at 383 K under vacuum prior to physisorption. The error in the BET surface areas is in the order of 15%.

Temperature-programmed reduction (TPR) was performed by H_2-consumption measurements in a conventional homemade TPR setup with TCD detector, after pretreatment in a He flow (99.996% pure) of 40 mL/min. Samples that were milled in the presence of CO_2 were pretreated by heating at 600 K/h up to 773 K, which was held during 15 min. For all other samples a temperature program was used identical to the one used for TGA. During reduction, a H_2/Ar mixture (2:1; total flow: 20 mL/min; Praxair, purity: 99.999%) was used as a feeding gas and heating was at 300 K/h. Oxidation levels of Cu were determined from reduction patterns of both TGA and TPR. 100% of CuO reduction corresponds to the initial oxidation level of CuO, and 50% to the oxidation level of Cu_2O.

X-ray diffraction (XRD) patterns were recorded with an Enraf Nonius Curved Position Sensitive 120 (CPS 120) diffractometer using Cu Kα radiation. Crystallite sizes were determined from the widths of the diffraction lines by means of the Scherrer formula after correction for the instrumental broadening.

High-resolution transmission electron microscopy (TEM) and electron diffraction were performed using a Philips CM30UT electron microscope operated at 300 kV. In this microscope, EDX elemental analysis was carried out by means of a LINK EDX system. Some additional transmission electron microscopy and electron diffraction were carried out at 100 kV.

Pore size distributions were determined by Hg-porosimetry at pressures up to 400 MPa.

Surface averaged mean particle sizes were determined with a Coulter Multisizer.

Differential scanning calorimetry (DSC) traces were taken by means of a Perkin-Elmer DSC 7 at a heating rate of 600 K/h in an Ar flow.

Inductively coupled plasma−atomic emission spectroscopy (ICP-AES), using a multichannel Thermo Jarrel Ash ICAP 957 spectrometer, has been performed on all samples to determine the contamination levels due to the milling equipment (Fe, Cr, Ni). The contamination of the milled samples mainly consisted of Fe and was in general well below 1 at. %. Within the experimental error, Cu:Zn atomic ratios had remained unchanged during milling.

Differential dissolution was used for determination of the stoichiometry of separate phases. This method has been described in ref 22.

Methanol synthesis activity measurements were carried out in a glass tube reactor at a pressure of 2 bar. The amount of (unreduced) catalyst used for each run was 250 mg. The synthesis gas CO/H_2 (at a ratio of 1:2) was applied at a flow of 7.5 mL/min (standard conditions: 298 K and 1 bar). Reaction products were analyzed with a GC and detected by a flame ionization detector after passing though a methanizer containing a Ni catalyst held at a temperature of 723 K. Calibration was carried out to determine the sensitivities to the various reactants. Prior to synthesis, pretreatment in He and reduction in H_2 were carried out in-situ at a flow of 30 mL/min following the thermal treatment described for TGA.

Results and Discussion

1. Cu, Cu_2O, and CuO. Powders of Cu, Cu_2O, and CuO were mechanically milled during 200 h under vacuum, in synthetic air and in carbon dioxide. Milling of Cu under vacuum was not considered, as Cu powder tends to coalesce during milling due to its high ductility. A significant broadening of the diffraction peaks is observed in the XRD patterns of all milled samples (Figures 1−3). This peak broadening is typical of all mechanically milled materials and indicates a reduction of the crystallite size due to disordering and microstructural refinement. In Figures 1−3, a subtraction of the background has been carried out for better recognition of the diffraction peaks, except for CuO milled in CO_2. This latter sample has undergone almost complete amorphization. During milling, broadening of the particle-size distributions is observed for all

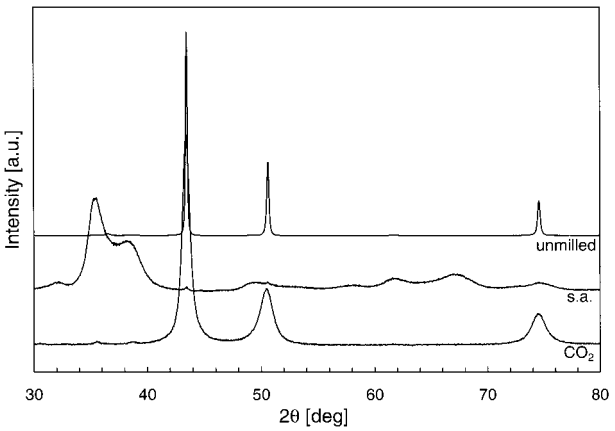

Figure 1. XRD patterns of unmilled and milled Cu.

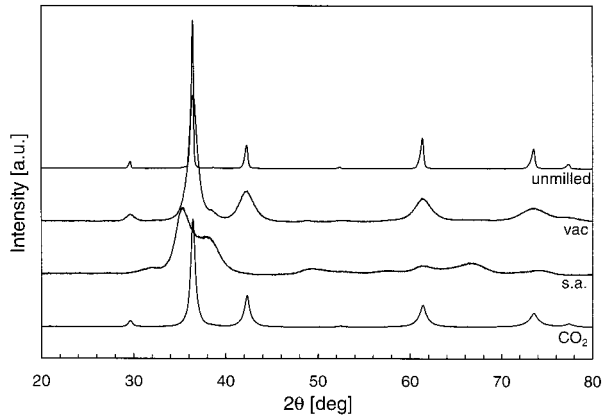

Figure 2. XRD patterns of unmilled and milled Cu_2O.

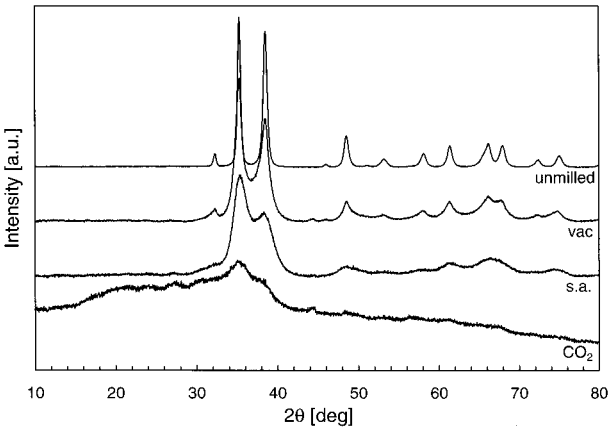

Figure 3. XRD patterns of unmilled and milled CuO.

samples, the mean particle size (8−16 μm) being slightly smaller for milled samples.

1.1. Mechanochemical Reactions. Three different types of reactions are observed during the milling experiments, as can be concluded from the XRD patterns and from the oxidation levels (%CuO) that are determined from H_2-reduction data (Table 1): oxidation, carbonate formation, and reduction. The error in the TGA data is approximately 1%, in the TPR data it is about 4%.

Oxidation: The original peaks in the XRD patterns of the Cu and Cu_2O samples that were milled in synthetic air have almost completely disappeared in favor of a pattern of CuO (Figures 1 and 2). In the Cu and Cu_2O samples that were milled under vacuum or in CO_2, the original XRD peaks are retained, indicating the absence of a chemical reaction during milling.

TABLE 1: Analytical Data of Unmilled and Milled Cu, Cu_2O, and CuO Samples

sample	milling conditions	mean particle size [μm]	% CuO reduced (TGA)	% CuO reduced (TPR)	$T_{max\ reduction}$ (TGA) [K]
Cu	unmilled	11.7	5.4		402
Cu	synth. air	9.3	99.6		408
Cu	CO_2		1.2		368
Cu_2O	unmilled	8.5	50.1		515
Cu_2O	vacuum		52.2		408
Cu_2O	synth. air		108.3	100	406
Cu_2O	CO_2	11.6	49.9		397
CuO	unmilled	16.2	101.2	100	414
CuO	vacuum	10.7	95.4	85	404
CuO	synth. air	10.0	103.6		410
CuO	CO_2	13.6	97.2	98	407

Complete oxidation to CuO of the Cu and Cu_2O samples that were milled in synthetic air can also be concluded from the oxidation levels.

Carbonate Formation: For the CuO sample that has been milled in CO_2, decomposition into CuO and CO_2 is observed by TGA-MS around 589 K. It was determined that, during milling, 65.4% of the CuO had been transformed to $CuCO_3$. However, no $CuCO_3$ diffraction lines can be observed (main peaks at 24.7°, 29.9°, and 33.9°). The halo that is observed in the XRD pattern (Figure 3) must therefore be due to the formation of amorphous Cu carbonate. After decomposition at 773 K, porosity is observed with pore diameters of around 100 nm.

Reduction: As metallic Cu is always covered with a surface-oxidation layer, the as-received sample has a nonzero oxidation level. As the oxidation level has decreased after milling in CO_2, reduction of the surface passivation layer has apparently occurred. For the Cu_2O sample milled in CO_2, no such effect is observed in the reduction data. However, during pretreatment a weight loss of about 0.27% of the total mass after reduction is observed at 418 K, which could be caused by decomposition of an unstable copper carbonate species. The H_2-reduction data of CuO milled in CO_2 suggest that, except for carbonate formation, some reduction takes place during milling as well.

Reduction can also be observed during milling of CuO under vacuum, which follows from both the TGA and the TPR data. It has to be remarked that this sample was unusually contaminated with a comparatively large amount (in this case in total around 9%) of metallic Fe and Cr, due to a different pretreatment of the milling vial. The contamination has been corrected for in Table 1 by subtraction of its contribution to the total weight.

1.2. H_2-Reduction Patterns and Structure after Reduction. As compared to their unmilled precursors, all milled samples show decreased reduction temperatures, which is especially apparent for Cu_2O. The depression of the reduction temperature can be explained by roughening of the surface due to the creation of matrix defects and of O-vacancies.[23] Very steep reduction profiles are found for all CuO samples and for the Cu and Cu_2O samples that were milled in synthetic air. Reduction is accompanied by an additional temperature rise of a few degrees, as observed by a thermocouple positioned next to the sample in the thermobalance, indicating that reduction proceeds very quickly and exothermically (ΔH^0 for CuO reduction is of the order of -10^5 J/mol). This can be attributed to insufficient transport of excess heat and autocatalysis by freshly reduced Cu^0.[24] The other samples have much broader reduction profiles, which can be explained by their lower oxidation levels.

For all samples that were milled in CO_2, the reduction peak is located at a relatively low temperature, also compared to other

TABLE 2: Cu^0 and BET Surface Areas after H_2 Reduction of Unmilled and Milled Cu, Cu_2O, and CuO Samples

	unmilled	vacuum	synth. air	CO_2
Cu^0 surface area (N_2O) [m^2/g]				
Cu	0.6		2.1	0.5
Cu_2O	0.4	2.1	1.9	0.4
CuO	2.2	15.4	19.2	10.0
BET surface area (N_2) [m^2/g]				
CuO	4.9	28	31	17

TABLE 3: Analytical Data of Unmilled and Milled ZnO Samples

milling conditions	mean particle size [μm]	BET surf. area [m^2/g]	[%] metallic contamination
unmilled	15.0	3.0	0.05
vacuum	11.6	4.2	1.2
synth. air	13.0	6.0	0.5
CO_2	10.5	8.4	0.1

milled samples. Apparently, both the presence of CO_2 and a low O_2 partial pressure during milling give rise to an easily reducible structure, which is also indicated by the lower oxidation levels of the Cu and CuO samples after milling. The decreased reduction temperature of the CuO sample milled under vacuum may also be attributed to a larger number of O-vacancies at the surface (and thus to the presence of Cu^0) facilitating initiation of the reduction. The TPR peak maxima that have been determined follow the trends of the TGA peak maxima.

The Cu^0 specific surface areas (determined by N_2O chemisorption) and BET surface areas (both after reduction) are summarized in Table 2. The surface areas of the Cu and Cu_2O samples that were milled in synthetic air are slightly larger than those of their unmilled precursors, whereas of all milled CuO samples they are highly increased. This increase cannot only be attributed to the decrease in particle size, but is also due to surface roughening.

A ratio of about 1.8 between the BET surface areas and the Cu^0 specific surface areas is observed for the reduced CuO samples, where similar values for the two different methods are expected. The same ratio is observed when CO_2 is taken as a probe molecule for physisorption instead of N_2, excluding a different orientation of the physisorbed N_2 molecule. No satisfying explanation for this factor has yet been found. However, the two methods are fundamentally different, employing different probe molecules and physical/chemical principles.

2. ZnO. *2.1. Defect Formation.* After milling of ZnO under vacuum, in synthetic air, and in CO_2, the white color of ZnO had changed to olive-green (vacuum), yellow-green (synthetic air), and yellow (CO_2). The XRD patterns of the samples do not reveal peak shifts, indicating that the lattice parameters of all milled ZnO samples have remained unchanged by milling (except for the typical line broadening). A small amorphous halo was observed for ZnO milled in CO_2. BET areas increase after milling (see Table 3), but at most with a factor of 3 for ZnO milled in CO_2. No porosity was observed after milling under vacuum or in synthetic air.

The color changes have been observed by others in milled ZnO as well.[25] Contamination by the milling equipment is clearly limited (Table 3) and cannot be the explanation. Color centers can be formed by irradiation[26] but are commonly found after a high-temperature treatment at around 1500 K and are generally explained to be due to oxygen vacancies. The number of oxygen vacancies is significantly higher after a thermal treatment in N_2 than in O_2.[27] Milling under vacuum will also result in the formation of oxygen vacancies and give a higher number than milling in synthetic air. Alternatively, milling in synthetic air could also result in a limited amount of interstitial oxygen. As the error in the ICP measurements is around 2%, the exact defect concentration is too small to be detected by means of this technique.

2.2. Carbonate Formation. During milling of ZnO in CO_2, about 13.3% of $ZnCO_3$ has been formed. Decomposition into ZnO and CO_2 is observed by TGA at around 558 K. As ZnO does not reduce under H_2 at these relatively low temperatures, both the extent of decomposition and the decomposition profile are observed to be independent of the atmosphere (either inert or reductive). After decomposition at 623 K, the amorphous halo has disappeared from the XRD pattern, the BET area has increased to 18.8 m^2/g, and a significant number of mesopores with a pore diameter of around 5 nm was detected. As no change in mean particle size has taken place during decomposition, the higher BET area after decomposition thus is entirely due to porosity.

3. Cu/ZnO, Cu_2O/ZnO, and CuO/ZnO Milled in a Vacuum or Synthetic Air. *3.1. Oxidation and Reduction through an Intermediate Structure.* Analytical data of Cu/Zn oxide mixtures that have been milled under vacuum or in synthetic air are summarized in Table 4. The H_2-reduction data can be compared to the data on unmilled and milled Cu samples that are given in Table 1. ZnO is assumed to remain unreduced under H_2 at the applied conditions. Both oxidation and reduction during milling can be observed: in synthetic air, Cu/ZnO and Cu_2O/ZnO are almost entirely oxidized to the level of CuO/ZnO, whereas by milling under vacuum the oxidation levels of Cu_2O/ZnO and CuO/ZnO decrease. The TGA oxidation levels are well reproducible within approximately 3%; the TPR errors are about 5%.

XRD patterns (Figure 4) also indicate the occurrence of mechanochemical reactions, but in a more complex way. All patterns show broadened diffraction peaks, typical of milling. The diffraction pattern of ZnO can be clearly identified for all samples. Between, some diffraction peaks characteristic of Cu, Cu_2O, and CuO can be observed with different intensities. These peaks are labeled in the figure for easier recognition.

In Cu/ZnO/s.a. (synthetic air) and in Cu_2O/ZnO/s.a. (Figure 4, traces a and c) some CuO can be observed indicating oxidation, but especially Cu_2O diffraction peaks can be clearly identified. In Cu_2O/ZnO/s.a., these Cu_2O peaks are unusually large relative to the ZnO peaks as compared to unmilled Cu_2O/ZnO. The ratio of the intensity of the (200) Cu_2O peak to the other crystalline peaks is about 8 times as large as compared to this ratio in the unmilled mixture. Even when the peak intensity is compared to the total XRD signal, i.e., including the background contribution, its size is still more than 3 times as large as in the unmilled mixture. The presence of Cu_2O is even more remarkable when it is considered that nearly complete oxidation to the level of CuO has occurred, so only a small fraction of Cu_2O is to be expected. One explanation may be a specific orientation of Cu_2O crystals, but as both the (200) and the (220) peaks of the cubic crystal are well represented this is not very probable. It is more likely that Cu_2O is well dispersed onto the ZnO, which is also indicated by the broad diffraction peaks. This (intermediate) state may even partially consist of ZnO and is probably the configuration in which further oxidation to CuO occurs. According to ref 1, Cu^+ may substantially dissolve into the ZnO lattice, in contrast to Cu^{2+}. In Cu_2O/ZnO/s.a. the Cu_2O peaks eventually disappear after more than 400 h of milling due to total oxidation to CuO.

The opposite is the case for CuO/ZnO/vac (Figure 4d), in

TABLE 4: Analytical Data of Cu-, Cu_2O- or CuO-, and ZnO-Containing Samples Milled under Vacuum or in Synthetic Air

sample	milling conditions	% reduced CuO (TGA)	% reduced CuO (TPR)	$T_{max.\ reduction}$ (TGA) [K]	max $T_{reduction}$ (TPR) [K]	mean $T_{reduction}$ (TPR) [K]
Cu/ZnO	synth. air	104.9	107	432	470, 492	484
Cu_2O/ZnO	vacuum	43.7	45	383	431	435
Cu_2O/ZnO	synth. air	94.4	98	414,[a] 442	463, 483	480
CuO/ZnO	vacuum	91.0	93	412[a]	457	459
CuO/ZnO	synth. air	105.7	103	409[a]	433, 446	443

([a]Explained in text.)

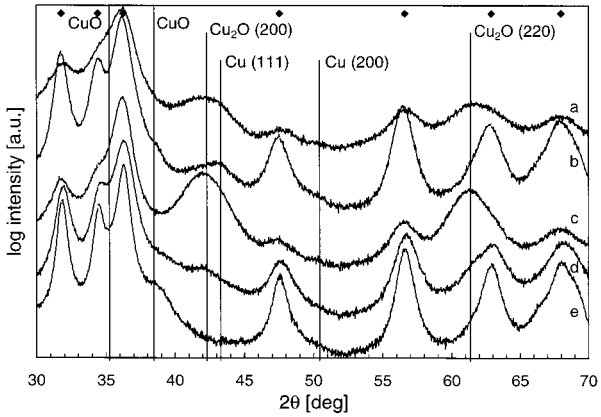

Figure 4. XRD patterns of milled (a) Cu/ZnO/s.a., (b) Cu_2O/ZnO/vac, (c) Cu_2O/ZnO/s.a., (d) CuO/ZnO/vac, and (e) CuO/ZnO/s.a. The patterns are plotted on a logarithmic scale. ZnO peaks are represented by ♦.

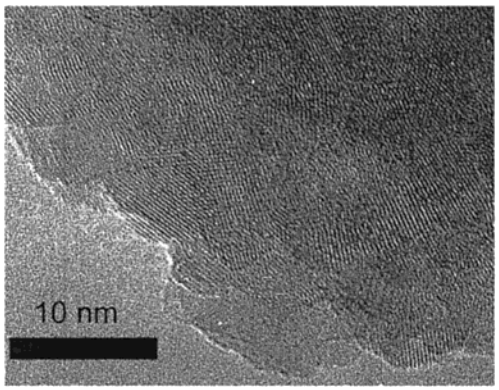

Figure 5. TE micrograph of Cu_2O/ZnO milled in synthetic air.

which both Cu_2O and a shoulder of CuO are visible. In Cu_2O/ZnO/vac (Figure 4b) not only Cu_2O but also Cu and a small shoulder of CuO can be seen. Disproportionation of Cu_2O into Cu and CuO has apparently taken place. As at shorter milling times CuO is more clearly visible, whereas Cu cannot yet be observed, a CuO structure is apparently formed first, which subsequently reduces to Cu. This would be in agreement with what was found in section 1.2, where reduction of pure CuO under vacuum has been observed but no reduction of pure Cu_2O, making this mechanism more probable than direct reduction of Cu_2O to Cu.

As can be expected, in the pattern of CuO/ZnO/s.a. (Figure 4e) only ZnO and (shoulders of) CuO are visible. This clearly indicates that no reduction or oxidation has taken place in this sample.

By means of electron diffraction, the same *d* spacings are observed as those found by XRD. Diffuse rings with some bright spots observed in Cu_2O/ZnO/s.a. indicate the presence of nanocrystalline material. With TEM carried out on CuO/ZnO/vac, some small crystallites with a size of around 10 nm can be observed at the edge of the particles. High-Resolution TEM measurements on Cu_2O/ZnO/s.a. (Figure 5) confirm that most of the material is nanocrystalline rather than amorphous, with crystallites between 2 and 8 nm. Crystallites that are situated on the edge of the particle appear entirely crystalline and do not exhibit an amorphous layer. The crystallite sizes scale well with the sizes that were determined from the X-ray diffraction lines, which are 6 nm for ZnO in CuO/ZnO/vac, and 3 nm (Cu_2O) and 5 nm (ZnO) for Cu_2O/ZnO/s.a. EDX shows that the composition is more or less homogeneous throughout the sample, independent of the crystallite size.

ZnO apparently serves as a support on which Cu oxides can be stabilized, as Cu_2O-like intermediates have not been observed in similar experiments on Cu and Cu oxides without ZnO (section 1). The direction of the net reaction is dependent on the amount of oxygen present in the sample and the O_2 partial pressure in the milling vial. It may be noted that ZnO is an n-type semiconductor that can easily form an excess of interstitial Zn^{2+} and e^-, whereas Cu_2O is a p-type forming a deficit of Cu^+. Oxygen ions may then be built into the Cu_2O matrix, being compensated in charge by Zn^{2+}. Although speculative, this mechanism would explain both the high intensity of the (200) Cu_2O peak and the oxidation and reduction reactions. The presence of superstoichiometric O in Cu_2O thus explains the high oxidation level, while diffraction lines of Cu_2O remain visible.

Differential dissolution (DD) of Cu/ZnO/s.a. and Cu_2O/ZnO/s.a. shows simultaneous dissolution of Cu and Zn at constant stoichiometry. Consequently, very good contact exists between Cu and Zn and even mixed oxide compounds may have been formed. For CuO/ZnO/s.a., a good mixture of Cu and Zn is observed as well, since DD does not show presence of pure Cu or Zn containing phases. However, the Cu concentration increases over 5% during solution of this sample, which indicates that this sample is slightly less homogeneous.

3.2. H_2-Reduction Patterns and Catalyst Structure after Reduction. Reduction of Cu/Zn mixtures indicates the presence of various reducible CuO species. The TPR hydrogen consumption patterns (Figure 6) are positioned at higher temperature than the TGA reduction profiles (Figure 7) and are broader. This is attributed to a higher heating rate for TPR as well as a better heat transport from the sample. Various distinct surface species can be observed from the TPR patterns, of which the principal peak maxima are given in Table 4. However, it has not been possible to assign different chemical bindings to these species. Therefore, mean reduction temperatures have also been given here. The use of mean reduction temperatures instead of peak maxima is more appropriate in view of the complex TPR patterns observed, but does not change the overall conclusion of these experiments. The mean values are generally positioned at higher temperatures than the individual peak maxima due to strong tailing. All trends and relative peak positions in the TPR reduction patterns are in accordance with the TGA data.

The low reduction temperature (for both reduction patterns) of Cu_2O/ZnO/vac confirms the presence of a significant amount of Cu^0 catalyzing the reduction of mainly Cu_2O.

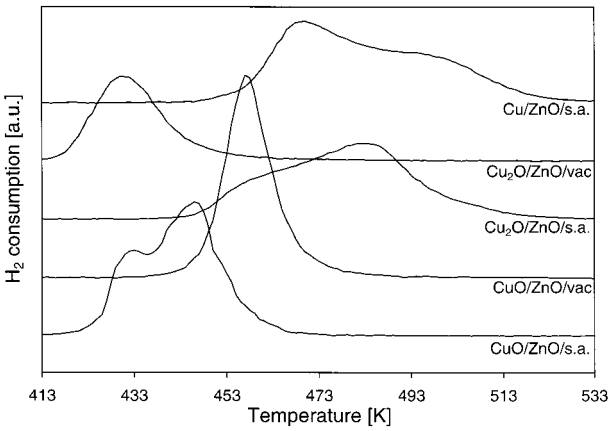

Figure 6. TPR H_2-consumption patterns of milled Cu/Zn oxide mixtures.

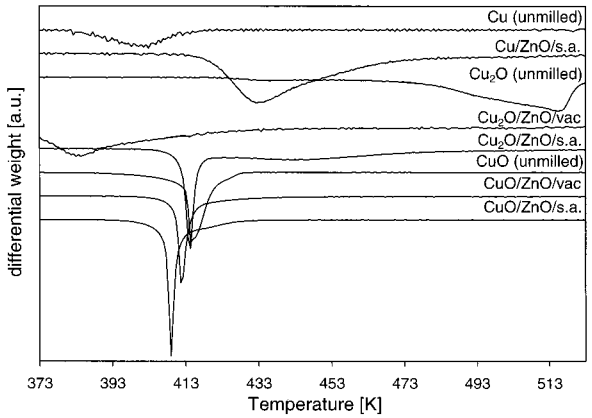

Figure 7. TGA reduction profiles of milled Cu and Cu/Zn oxide mixtures.

For TGA, the first reduction peak of Cu_2O/ZnO/s.a. and the reduction profiles of both CuO/ZnO samples, indicated with an asterisk in Table 4, are very steep and positioned at relatively low temperatures. Reduction is accompanied by an additional temperature rise of a few degrees, as was similarly the case for CuO samples in section 1.2, indicating that reduction proceeds very quickly and exothermically. In these samples, the presence of a relatively easily reducible CuO species is assumed, with freshly reduced Cu^0 autocatalytically enhancing further reduction.[24] TPR gives intermediate reduction temperatures for CuO/ZnO samples.

The second (TGA) reduction peak of Cu_2O/ZnO/s.a. and the reduction profile of Cu/ZnO/s.a. are much broader and positioned at a higher temperature. The TPR patterns of these samples are also positioned at the highest temperatures. The higher reduction temperature of this species is associated with closer intimacy with ZnO and presence of Cu_2O. Comparison of XRD patterns and TPR reduction profiles indicate the relation between occurrence of Cu_2O and an increase in the reduction temperature. Moreover, higher reduction temperatures for copper samples milled without ZnO have not been observed (Table 1). This delaying effect of ZnO on the reduction of CuO has also been found to be accompanied by the existence of stable Cu_2O by Ruggeri et al.[28]

After reduction in H_2, the XRD patterns show narrower diffraction peaks of metallic Cu and ZnO as compared to the as-milled samples, indicating larger crystallites. TEM measurements carried out on CuO/ZnO/vac after reduction and passivation with N_2O also show a slight increase in crystallite size (10 nm and larger) as compared to sizes observed prior to reduction. This is not unexpected after reductive, i.e., hydrothermal treatment.

All samples show enhanced surface areas as compared to copper (oxides) and ZnO that have been milled separately. These data are shown in Table 6 and will be further discussed in section 5.

4. Cu/ZnO, Cu_2O/ZnO, and CuO/ZnO Milled in the Presence of CO_2. *4.1. Carbonate Formation.* XRD patterns of Cu/Zn oxide mixtures that have been milled in the presence of CO_2 are shown in Figure 8. A small halo can be observed, indicating material that is amorphous or consists of very small crystallites.

While carbonates are formed during milling of CuO or ZnO in CO_2 (sections 1 and 2), Cu/Zn oxide mixtures also give rise to the formation of carbonates under these conditions. DSC traces are shown in Figure 9, indicating decomposition of these carbonates. Various carbonate species are formed of which mean decomposition temperatures and decomposition enthalpies are given in Table 5. Most mixed carbonates that are formed decompose at higher temperatures and have higher decomposition enthalpies than carbonates formed in CuO/CO_2 (664 K at 421 kJ/mol) or ZnO/CO_2 (578 K at 214 kJ/mol). This indicates a higher stability of the CO_3^{2-} anion for mixed Cu/Zn samples and intimate contact between Cu and Zn.

The amount of carbonate formed is higher for high CO_2 partial pressures (i.e., for milling in CO_2 instead of s.a.+CO_2), as well as for high Cu oxidation levels. Moreover, both decomposition temperatures and decomposition enthalpies are higher for high oxidation levels, indicating formation of a more intimate Cu/Zn mixture. Apparently, in the presence of CO_2, good mutual solubility exists between CuO and ZnO, and poor mutual solubility between Cu or Cu_2O and ZnO. This is supported by observations in section 1 that carbonates can be formed in CuO rather than in Cu and Cu_2O. Milling of mixtures of Cu/ZnO or Cu_2O/ZnO in CO_2 will therefore initially give rise to formation of $ZnCO_3$ rather than $CuCO_3$ or mixed carbonates. Whereas solubility of CuO in ZnO is usually poor (about 2−4%),[29] Yurieva et al. have also observed a significant increase for anion-modified ZnO.[30]

4.2. Oxidation and Reduction. Oxidation levels (Table 5) have been determined in two ways: by combination of DSC and TGA data, and by determination of H_2 consumption (TPR), with errors in both methods of approximately 5%. During milling, an increase of the oxidation levels of Cu/ZnO and Cu_2O/ZnO has occurred in a mixture of CO_2 and synthetic air. In CO_2 alone, oxidation levels of Cu_2O/ZnO and CuO/ZnO have decreased to a further extent than during milling of these mixtures under vacuum (Table 4).

In the XRD patterns (Figure 8), characteristic diffraction peaks of Cu, Cu_2O, and CuO are labeled for easier recognition. No Cu_2O or CuO peaks can be observed, although a CuO shoulder is visible in most patterns (b−f). Apparently, CuO has partially dissolved into the ZnO matrix, is mostly amorphous, or has crystallite sizes that are too small to be detected by XRD.

In the patterns of Cu/ZnO (a,b) and in $Cu_2O/ZnO/CO_2$ (c), a significant amount of Cu^0 is visible. As the oxidation level of $Cu/ZnO/CO_2$ is low (Table 5), this is no surprise for (a) ($Cu/ZnO/CO_2$). In CO_2 and s.a. (b), Cu in the Cu/ZnO mixture oxidizes to CuO and partially dissolves into the ZnO matrix forming a mixed carbonate. The remainder of Cu remains in metallic form. For $Cu_2O/ZnO/CO_2$ (c), a significant reduction of Cu_2O to Cu^0 occurs due to the low O_2 partial pressure. Apparently, Cu_2O splits into Cu^0, which is visible in the XRD pattern, and a small amount of CuO. The CuO may dissolve

TABLE 5: Analytical Data of Cu-, Cu_2O- or CuO-, and ZnO-Containing Samples Milled in the Presence of CO_2

sample	milling conditions	% CO_3^{2-}	mean $T_{decomp.}$ CO_3^{2-} [K]	ΔH_{decomp} [kJ/mol CO_3^{2-x}]	% CuO (DSC/TGA)	% CuO (TPR)	max $T_{reduction}$ (TPR) [K]	mean $T_{reduction}$ (TPR) [K]
Cu/ZnO	CO_2	26.8	612	335	6	5	390, 400	402
Cu/ZnO	s.a.+CO_2	20.8	676	528	63	68	408, 423	421
Cu_2O/ZnO	CO_2	31.4	610	345	36	34	395, 409	405
Cu_2O/ZnO	s.a.+CO_2	33.4	743	622	88	94	414, 425, 439	429
CuO/ZnO	CO_2	44.4	732	577	86	81	420, 431	423
CuO/ZnO	s.a.+CO_2	33.6	709	613	92	99	424, 437	427

TABLE 6: Cu^0 and BET Surface Areas after H_2 Reduction of Samples in Which Cu and Zn Precursors Were Milled Separately and Subsequently Physically Mixed ("+"; p.m.) and Milled Together ("/")

	unmilled	vacuum	synth. air	CO_2	s.a.+CO_2
Cu^0 area					
Cu + ZnO p.m.	0.2	<0.1	0.5	0.2	
Cu/ZnO		0.4	7.2	17	31
Cu_2O + ZnO p.m.	0.1	0.5	0.5	0.1	
Cu_2O/ZnO		6.4	8.8	36	44
CuO + ZnO p.m.	0.6	3.9	4.8	2.5	
CuO/ZnO		11.1	11.3	42	37
BET area					
CuO + ZnO p.m.	3.5	10.2	12.3	18.3	
CuO/ZnO		29	24	69	59

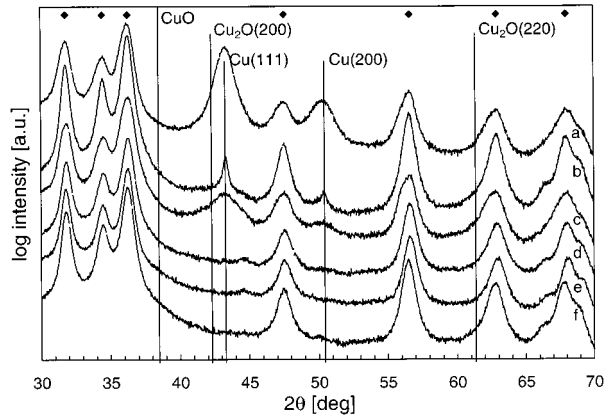

Figure 8. XRD patterns of milled (a) Cu/ZnO/CO_2, (b) Cu/ZnO/s.a+CO_2, (c) Cu_2O/ZnO/CO_2, (d) Cu_2O/ZnO/s.a.+CO_2, (e) CuO/ZnO/CO_2, and (f) CuO/ZnO/s.a.+CO_2. The patterns are plotted on a logarithmic scale. ZnO peaks are represented by ♦.

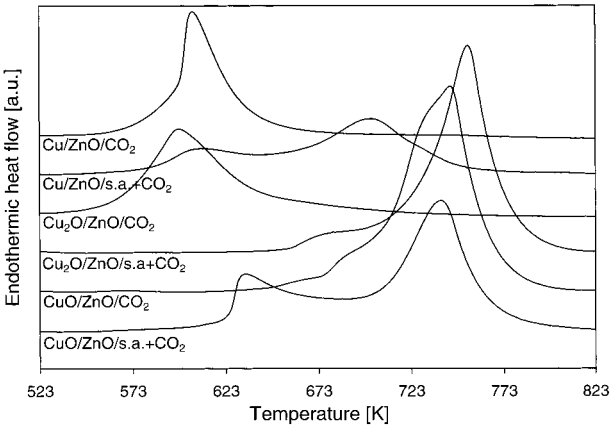

Figure 9. DSC traces showing decomposition of milled Cu/Zn carbonate mixtures.

into the ZnO matrix, forming a mixed carbonate. I.e. Cu_2O species are unstable under the applied conditions. The same disproportionation has been observed for this mixture during milling under vacuum (section 3), although to a much lesser extent. While ZnO promotes reduction, the presence of a Zn

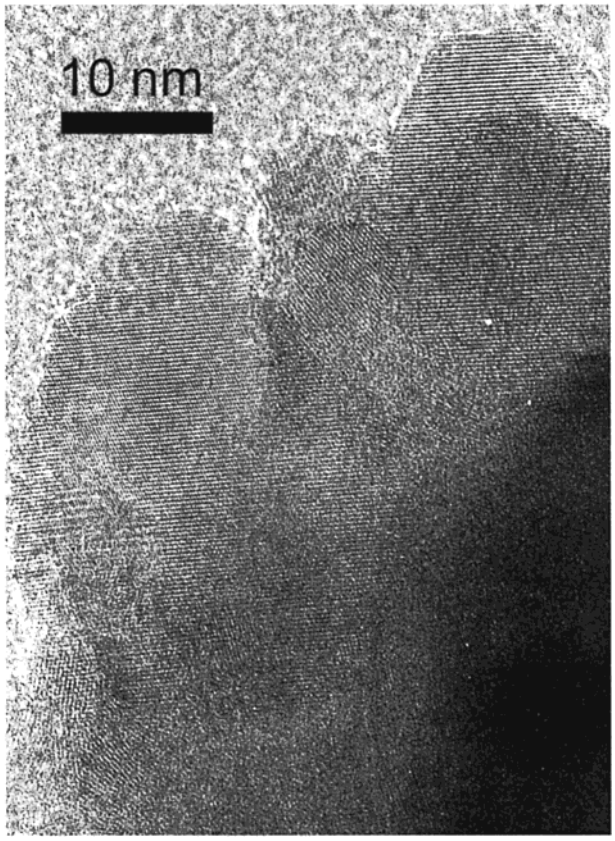

Figure 10. TE Micrograph of Cu_2O/ZnO milled in synthetic air + CO_2.

carbonate appears to be even more effective for reduction of Cu_2O. Although only a limited amount of Cu species may have dissolved into the ZnO matrix for both Cu/ZnO/CO_2 and Cu_2O/ZnO/CO_2, decomposition temperatures and enthalpies are still higher than for ZnO/CO_2 alone. This indicates that a modification of the ZnO matrix has still occurred for these two samples.

TEM measurements have been carried out on Cu_2O/ZnO/CO_2 and Cu_2O/ZnO/s.a.+CO_2 (Figure 10). Crystallite sizes can be observed between 3 and 20 nm, which is larger than observed in the oxidic mixtures. For both materials, the same diffraction lines are observed as by XRD, and crystallite sizes scale well with those determined from the X-ray diffraction lines, that are 7 nm (Cu) and 8 nm (ZnO) for Cu_2O/ZnO/CO_2, and 11 nm (ZnO) for Cu_2O/ZnO/s.a.+CO_2. EDX on both materials shows the presence of both Cu-rich and Zn-rich particles. In general, particles show a Cu-rich fraction on the edge, and a Zn-rich fraction in the bulk.

Differential dissolution shows constant stoichiometry for CuO/ZnO/CO_2, indicating a good homogeneity of the particles. Homogeneity is enhanced with respect to the CuO/ZnO/s.a. sample (section 3.1) and supports the view of enhanced mixing by anion-modification. Cu_2O/ZnO/s.a.+CO_2 is also a homogeneous sample, although a small fraction of a separate Cu phase can be observed. Cu_2O/ZnO/CO_2, on the other hand, is quite

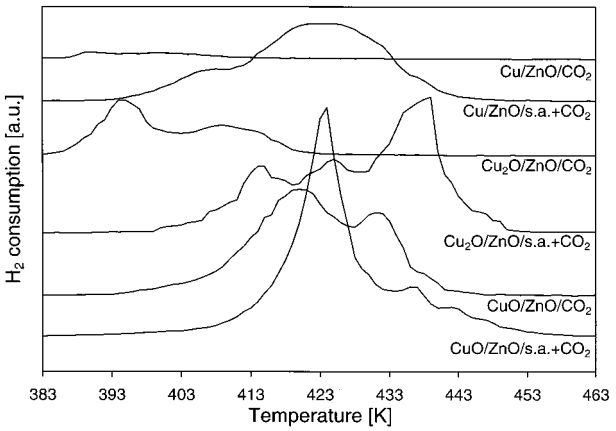

Figure 11. TPR H_2-consumption patterns of milled Cu/Zn carbonate mixtures.

inhomogeneous with the Cu fraction rising during solution of the sample from 0.12 to 0.5. This may indicate a Zn-rich surface, but more likely the existence of two separate phases, i.e., an easily soluble Zn-rich phase and a harder soluble Cu-rich phase. This supports the observation of disproportionation of Cu_2O into two separate species—Cu and CuO.

4.3. H_2-Reduction Patterns and Catalyst Structure after Reduction. When reduction is carried out for samples that have not been fully decomposed, e.g., when pretreatment is carried out up to 523 K, a higher H_2 consumption is detected than expected based on the measured oxidation level. In that case a reverse watergas shift reaction ($CO_3^{2-} + 2H_2 \rightarrow CO + 2H_2O + 2e^-$) takes place. This has been observed in Cu/Zn oxides milled in CO_2 but not in CuO/CO_2, indicating that this reaction is promoted by the presence of ZnO, and thus that active catalysts have been produced.

To measure only the effect due to reduction, decomposition was carried out (at 773 K) prior to H_2-consumption measurements by TPR. Several CuO species could be detected (Figure 11). Similar to the oxidic mixtures (section 3.2), mean temperatures for the reduction patterns have been determined in addition to the principal peak maxima (Table 5). Again, higher values for the reduction temperatures can be observed for samples that decompose at higher temperatures. Combined with their higher oxidation levels, this implies a more intimate contact between Cu and Zn.

TEM measurements on reduced $Cu_2O/ZnO/s.a.+CO_2$ (Figure 12) show that the morphology is similar to that of the unreduced material, with comparable crystallite sizes. Again, some Cu-rich particles are observed by means of EDX. Metallic Cu is clearly visible by means of electron diffraction, but diffraction lines of Cu_2O and CuO can also be observed. Apparently, some reoxidation of the sample has occurred during storage and handling.

5. Surface Areas. After reduction, Cu^0 specific surface areas of all milled samples discussed here are strongly increased as compared to their unmilled precursors (Table 6). When Cu(oxides) and ZnO are milled together under vacuum or in synthetic air, both Cu^0 specific surface areas and BET areas are increased by more than 1 order of magnitude as compared to separately milled mixtures. A previously investigated Cu/ZnO sample milled under vacuum,[6] showing both low Cu^0 area and low BET surface area, has also been included here. The high surface areas obtained by simultaneous milling of Cu and Zn samples could be attributed to a larger Cu(oxide) dispersion due to the presence of or interaction with ZnO during milling.

Figure 12. TE Micrograph of Cu_2O/ZnO milled in synthetic air + CO_2, after reduction in H_2.

Another factor may be stabilization of dispersed Cu^0 by ZnO after reduction.

All milled Cu/ZnO samples have broad particle-size distributions with an average diameter of around 10 μm. No clear relation exists between particle size and milling atmosphere or surface area. Still, surface areas are further increased when milling is carried out in the presence of CO_2. For some samples this can be attributed to a better contact between Cu and Zn. This gives rise to higher Cu^0 dispersion after reduction. On the other hand, surface areas are also increased for samples milled in the presence of CO_2 in which mixing of Cu and Zn is relatively poor. Porosity after decomposition and reduction may provide an additional explanation for this effect. After decomposition at 723 K, e.g., mesopores with 20 nm diameter could be detected, providing a more effective support for the copper phases.

In general, surface areas are enhanced by the occurrence of mechanochemical reactions, resulting in a high dispersion as well as good Cu−Zn contact. When solid solubility is good, mechanical milling can enhance mixing. Mechanical properties such as ductility, notably of metallic Cu (Cu/ZnO/vac[6]), can limit the surface area.

6. Catalytic Activity. Methanol synthesis activity measurements have been carried out on almost all milled Cu/ZnO samples in CO/H_2 (1:2) at low pressure (2 bar) and are summarized in Table 7. Conversion at this pressure is low but the error in the activity data is moderate: in the order of 10%. At 523 K, the maximum (equilibrium) conversion rate under these (p,T) conditions is reached for some samples. These values are indicated with an asterisk and result clearly in lower values for the turnover frequency (TOF). The average value of 5.6 nmol/s scales very well with theoretically predicted values for these reaction conditions. Values that are found with equilibrium constants proposed by six different authors average 5.9(8) nmol/

TABLE 7: Methanol Synthesis Rate and Turnover Frequencies (TOF) for a CO/H_2 Mixture (1:2) at 2 Bar and a Flow of 7.5 mL/min

sample	milling conditions	rate (523 K) [nmol/s]	[10^{-6} molecules/(Cu^0site-s)] TOF (523 K)	TOF (498 K)	TOF (473 K)
Cu/ZnO	s.a..	3.1	76	-	
Cu/ZnO	CO_2	4.1	46	46	25
Cu/ZnO	s.a.+CO_2	5.4[a]	33[a]	45	33
Cu_2O/ZnO	vacuum	2.0	54	41	31
Cu_2O/ZnO	s.a.	2.8	56		
Cu_2O/ZnO	CO_2	5.3[a]	29[a]	40	25
Cu_2O/ZnO	s.a.+CO_2	5.9[a]	27[a]	38	30
CuO/ZnO	vacuum	2.9	45		
CuO/ZnO	s.a.	5.2	82		
CuO/ZnO	s.a.+CO_2	5.7[a]	32[a]	46	35
average			60	43	30

[a] Equilibrium conversion is reached at the applied conditions.

s.[31] This maximum rate is reached only with samples that have been milled in the presence of CO_2. For sub-equilibrium conversions, a roughly linear relation is observed between rate and Cu^0 area, which becomes apparent by more or less equal TOF. A tendency for a somewhat higher TOF is observed for samples that have been milled in the presence of oxygen compared to samples that have been milled without oxygen. The constant factor between average TOF (excluding the samples with maximum conversion) at the different temperatures indicates a constant increase in reaction rate at higher temperatures. Apparent activation energies E_a are of the same order for all samples and average 25 kJ/mol. The average values are slightly lower for samples that have been milled in the presence of oxygen (21 kJ/mol) as compared to the samples that were milled without oxygen (28 kJ/mol). However, considering the accuracy of the measurements, the difference found is not sufficient to propose different pathways (or active sites) for the two types of catalysts.

Catalyst deactivation occurs after prolonged exposure to reaction conditions. The observed deactivation is sharpest immediately after applying reaction conditions and flattens out after approximately 15 h. A slight increase in activity (3 to 10%) is observed after flushing at low temperature with He or after a new cycle of pretreatment and H_2 reduction, which implies a partially reversible deactivation. The irreversible part is especially apparent at higher temperatures and is accompanied by a decrease in Cu^0 surface area. After 100 hrs at 523 K, a decrease in activity of about 20 to 30% is found. This value scales well with the decrease in Cu^0 surface area of around 25% found at the same temperature at 1 bar by TGA after exposing the catalyst to the same mixture of reactants. Moreover, after reduction and changing the atmosphere from H_2 to CO/H_2 an extra weight decrease is observed, corresponding to an extra CuO reduction of 15%. This suggests that over-reduction occurs which leads to sintering of the Cu^0 surface and irreversible deactivation. The small amount of reversible deactivation can be explained by the occupancy of sites by adsorbed species, possibly methanol, water, or methoxy species (see below).

When deactivation rates of the various samples are compared, an inverse relation is found between deactivation and the rate of decrease of measured CO_2 at the beginning of methanol synthesis, i.e., after pretreatment and reduction. This provides a possible explanation for the over-reduction by CO (see above), as this leads to formation of CO_2. In cases where CO_2 partial pressure decreases rapidly, over-reduction does not play a significant role, and deactivation is less prominent.

As a side-product of the synthesis reaction, some methyl formate is detected at 523 K. As conversion to methyl formate was extremely low, in the order of a few percent of the amount of methanol, no quantitative analysis could be carried out. Methyl formate indicates the presence of a methoxy intermediate, and is observed on oxidized Cu species.[32] Possibly, active sites at the Cu−ZnO interface render Cu cationic in character and may thus stabilize methoxy species.[33] The methyl formate signal decreased after an extended period under reaction conditions, which is another indication for over-reduction.

Conclusions

Mechanochemical reactions are observed during mechanical milling of Cu oxides and ZnO in various atmospheres. A reduction of the crystallite size due to disordering and microstructural refinement is observed for all materials, and is typical of mechanical milling. Milling of Cu and Cu_2O results in oxidation to CuO when milling occurs in synthetic air. Milling of CuO results in partial reduction when carried out under vacuum and carbonate formation when carried out in CO_2. No carbonates are formed from Cu_2O nor does any reduction take place. Bivalent Cu is found to be required when CO_2 is to be built into a copper oxide matrix or for creating oxygen vacancies. Mechanical milling of ZnO results in a slightly higher surface area, probably due to surface roughening. A carbonate is formed when ZnO is milled in CO_2.

Milling of mixtures of Cu, Cu_2O or CuO and ZnO results in oxidation of Cu precursors when carried out in synthetic air and in reduction when carried out under vacuum. These mechanochemical reactions are promoted by the presence of ZnO. Formation of a Cu_2O-like intermediate well dispersed on ZnO has been observed, as well as several copper oxide species reducing at different temperatures. The Cu_2O reduces at higher temperatures than other Cu species.

When Cu(oxide)/ZnO mixtures are milled in the presence of CO_2, carbonates are formed resulting in intimate Cu−Zn mixtures. These carbonates can only be formed from bivalent Cu and Zn, and only Cu^0 and CuO are observed by XRD after milling. Anion-modification explains enhanced mixing of CuO and ZnO. Reduction is observed when milling is carried out in only CO_2, and Cu_2O is rendered unstable, reacting toward Cu and CuO. Oxidation occurs when milling is carried out in a mixture of CO_2 and O_2. As no Cu_2O intermediate on ZnO is observed in these samples, formation of this intermediate appears to be dependent on both oxidation level and carbonate concentration.

Upon reduction, milled oxidic samples possess much higher BET and Cu^0 surface areas than both unmilled mixtures and mixtures of the separately milled components. This latter effect is probably due to an increased dispersion of Cu^0 by ZnO after reduction. The highest surface areas are found for mixed carbonates, which can be explained by the intimate Cu−Zn mixtures as well as by a porous structure, both yielding high Cu dispersion upon reduction.

Reaction rates for methanol synthesis are roughly linearly dependent on Cu^0 surface area. Highest initial reaction rates are reached for Cu/Zn oxide mixtures milled in CO_2. Irreversible catalyst deactivation is due to sintering of Cu^0 particles, caused by over-reduction in the reaction mixture at 523 K. Reversible deactivation may be due to strongly adsorbed products or intermediates. Formation of intermediate methyl formate indicates stabilization of methoxy species on Cu sites with a cationic character.

Due to mechanochemical reactions, active surface areas are strongly increased. Atomic ratios of precursors can be well

controlled and no waste products are produced. The unconventional preparation reveals a different range of reactions that may occur in this system and gives a deeper insight in the catalytic system. These considerations render mechanochemical preparation an interesting alternative for catalyst preparation as well as for studying catalytic systems.

Acknowledgment. J. Elgersma is gratefully acknowledged for performing ICP experiments, W. E. Brower of the Marquette University at Milwaukee, MI, for TEM measurements, P. J. Kooyman of the National Centre for High Resolution Electron Microscopy, Delft University of Technology, Delft, The Netherlands, for performing electron microscopy investigations, and V. V. Malakhov of the Boreskov Institute of Catalysis at Novosibirsk, Russia, for performing differential dissolution measurements. C. Tuijn is acknowledged for critical reading of the manuscript. The authors thank the Dutch Foundation for Fundamental Research on Matter (FOM) for financial support.

References and Notes

(1) Klier, K. *Adv. Catal.* **1982**, *31*, 243.
(2) Waugh, K. C. *Catal. Today* **1992**, *15*, 51.
(3) Matsuhisa, T. *Catalysis, A Spec. Per. Report*, Vol. 12; R. Soc. Chem.: Cambridge, 1996; p 1.
(4) Waller, D.; Stirling, D.; Stone F. S.; Spencer, M. S. *Faraday Discuss. Chem. Soc.* **1989**, *87*, 107.
(5) Fujita, S.; Satriyo, A. M.; Shen, G. C.; Takezawa, N. *Catal. Lett.* **1995**, *34*, 85.
(6) Huang, L.; Kramer, G. J.; Wieldraaijer, W.; Brands, D. S.; Poels, E. K.; Castricum, H. L.; Bakker, H. *Catal. Lett.* **1997**, *48*, 55.
(7) Bakker, H.; Zhou; G. F.; Yang, H. *Prog. Mater. Sci.* **1995**, *39*, 159.
(8) Schaffer, G. B.; McCormick, P. G. *Appl. Phys. Lett.* **1989**, *55*, 45.
(9) Schaffer, G. B.; McCormick, P. G. *Mater. Sci. Forum* **1992**, *88*−*90*, 779.
(10) Tokomitsu, K. *Z. Phys. Chem.* **1994**, *183*, 443.
(11) Cocco, G.; Mulas, G.; Schiffini, L. *Mater. Trans. JIM* **1995**, *36*, 150.
(12) Mulas, G.; Loiselle, S.; Schiffini, L.; Cocco, G. *J. Solid State Chem.* **1997**, *129*, 263.
(13) Nikolov, J. Ph.D. Thesis. Australian National University, Canberra, Australia, 1997.
(14) Zazhigalov, V. A.; Haber, J.; Stoch, J.; Bogutskaya, L. V.; Batcherikova, I. V. *Stud. Surf. Sci. Catal.* **1996**, *101*, 1039.
(15) Zamar, F.; Tovarelli, A.; de Leitenburg, C.; Dolcetti, G. *Stud. Surf. Sci. Catal.* **1996**, *101*, 1283.
(16) Lin, G. I.; Samokhin, P. V.; Kaloshkin, S. D.; Rozovskii, A. Ya. *Kinet. Catal.* **1998**, *39*, 577.
(17) Herman, R. G.; Klier, K.; Simmons, G. W.; Finn, B. P.; Bulko, J. B.; Kobylinski, T. P. *J. Catal.* **1979**, *56*, 407.
(18) Pan, W. X.; Cao, R.; Roberts, D. L.; Griffin, G. L. *J. Catal.* **1988**, *114*, 440.
(19) Castricum, H. L.; Bakker, H.; Poels, E. K. *Mater. Sci. Forum* **1999**, *312*−*314*, 209.
(20) Castricum, H. L.; Bakker, H.; Poels, E. K. *Mater. Sci. Eng. A* **2001**, *304*−*306*, 418
(21) Brands, D. S.; Poels, E. K.; Krieger, T. A.; Makarova, O. V.; Weber, C.; Veer, S.; Bliek, A. *Catal. Lett.* **1996**, *36*, 175.
(22) Malakhov, V. V.; Vlasov, A. A. *Kinet. Catal.* **1995**, *36*, 460.
(23) Andreini, A. Private Communication.
(24) Tiernan, M. J.; Barnes, P. A.; Parkes, G. M. B. *J. Phys. Chem. B* **1999**, *103*, 338.
(25) Boily, S.; Alamdari, H.; Cross, G.; Joly, A.; van Neste, A.; Grütter, P.; Schulz, R. *Mater. Sci. Forum* **1997**, *235*−*238*, 993.
(26) Puff, W.; Brunner, S.; Mascher, P.; Balogh, A. G. *Mater. Sci. Forum* **1995**, *196*−*201*, 333.
(27) de la Cruz, R. M.; Pareja, R.; González, R.; Boatnes, L. A.; Chen, Y. *Phys. Rev. B* **1992**, *45*, 6581.
(28) Ruggeri, O.; Trifirò, F.; Vaccari, A. *J. Sol. State Chem.* **1982**, *42*, 120.
(29) Locmelis, S.; Binnewies, M. *Z. Anorg. Allg. Chem.* **1999**, *625*, 1578.
(30) Yurieva, T. M.; Plyasova, L. M.; Makarova, O. V.; Krieger, T. A. *J. Mol. Catal. A* **1996**, *113*, 455.
(31) Skrzypek, J.; Słoczyński, J. Ledakowicz, S. *Methanol Synthesis*; Polish Scientific Publishers: Warszawa, Poland, 1994; p 8.
(32) Clarke, D. B.; Lee, D.-L.; Sandoval, M. J.; Bell, A. T. *J. Catal.* **1994**, *150*, 82.
(33) Clement, M.; Zhang, Y.; Brands, D. S.; Poels, E. K.; Bliek, A. *Stud. Surf. Sci. Catal.* **2000**, *130*, 2123.